Effects of a 3-D, Aquatic Vegetation Patch on the Flow: a Numerical Approach

TAÍS NATSUMI YAMASAKI
Faculty of Engineering, Architecture and Urban Planning, and Geography
Federal University of Mato Grosso do Sul
Av. Costa e Silva, s/n, 79070-900
BRAZIL
taisnatsumi@gmail.com

GIOVANNI CANNATA, FRANCESCO GALLERANO
LUCA BARSI
Department of Civil, Constructional and Environmental Engineering
Sapienza University of Rome
Via Eudossiana, 18 00184
Rome, Italy
ITALY
giovanni.cannata@uniroma1.it

JOHANNES GÉRSON JANZEN
Faculty of Engineering, Architecture and Urban Planning, and Geography
Federal University of Mato Grosso do Sul
Av. Costa e Silva, s/n, 79070-900
BRAZIL
johannesjanzen@gmail.com

Abstract: - This numerical study investigated the effects of a vegetation patch on the flow of a channel. The numerical approach consisted of a CFD, 3-D model that applied the RANS equations to simulate the flow field, and the VOF model to represent the free surface. The patch altered the initial flow by inducing regions of reduced velocity in the patch wake (approximately 40% reduction), and regions of enhanced velocity around of the patch (approximately 16% increase), and these regions extended throughout the water depth. Also, the patch induced a small change of 3.83% in the water surface, in the streamwise direction.

Key-Words: -aquatic vegetation patch, steady wake, open channel, free surface, Computational Fluid Dynamics, Volume of Fluid, RANS

1 Introduction

The importance of aquatic vegetation can be recognized by the ecological services that it provides for a given system (i.e., natural channels), which includes the improvement of water quality by means of oxygen production and nutrient removal [1], habitat provision [2] and bank reinforcement [3]. The vegetation can also modify the patterns of particle sedimentation and erosion, thus shaping the morphology of a channel [4]. Such is the relevance of aquatic vegetation on its surrounding that it can be considered a river systems engineer [5].

Emergent vegetation, which presents the top of its canopy above the water surface, is usually organized as patches or agglomerates in rivers [6], and so experimental studies in laboratories have been traditionally using circular model patches to mimic vegetation [7][8][9]. Early studies considered a patch that was placed in a channel of much greater width than the diameter of the patch, and the flow coming upstream [10][11]. When the flow encountered the patch, part of the water was laterally diverted around it, accelerating, while another part flowed through the voids of the patch at a reduced velocity due to the resistance of the vegetation stems (Fig. 1). Because the patch acted as a porous media, this velocity reduction persisted for a given length behind the patch before the flow returned to its original condition [11]. Consequently, it was deduced that this region behind the patch, called steady wake, can encourage the deposition of nutrients and sediments rich in organic matter, and thus become a favored region for new vegetation growth. On the other hand, it was expected to occur the inverse around the patch, given that the high velocity inhibits the deposition of nutrients [12]. The ability of blocking the flow in a less or a greater degree depends on two characteristics of the patch: the frontal area per unit volume a, and the diameter D, which combined forms the non-dimensional parameter aD, known as flow blockage [7]. Low values of flow blockage indicate that the patch does not reduce the flow as much as patches with high values of flow blockage.

Based on the interactions between the patch and the flow, numerical studies explored the effects of more than one patch on the flow field and how the resultant velocity can be linked to deposition, erosion and consequent vegetation evolution [13][14]. Hydrodynamically, simulations of free surface flows in complex geometries can be carried out by depth-averaged models [15][16][17].The vegetation was represented distinctly: in the case of de Lima et al. (2015)[14], the patches were defined

as an arrangement of individual cylinder stems, similar to laboratory experiments; in the case of Kondziolka and Nepf (2014)[13], the vegetation was represented as a porous media, where a source term was employed. Both models were two-dimensional and did not account for sediment transport, but rather for an indirect measure of likely deposition based on regions of reduced velocity that were induced by the vegetation.

The approach based on depth-averaged flows is only valid when the fully three-dimensional representation of the motion is not needed. In this study, we present a 3-D, numerical model of a vegetated channel, in which the interactions between the flow and the vegetation patch were simulated by using Computational Fluid Dynamics (CFD). This study aims to be an initial step towards a model that will eventually couple sediment transport in the simulations and account for sediment bed evolution, and therefore build on the works of previous studies that used velocity to predict regions of vegetation growth [13][14]. To make the simulation closer to laboratory experiments [10][11], the patch was represented as an arrangement of cylinder stems.

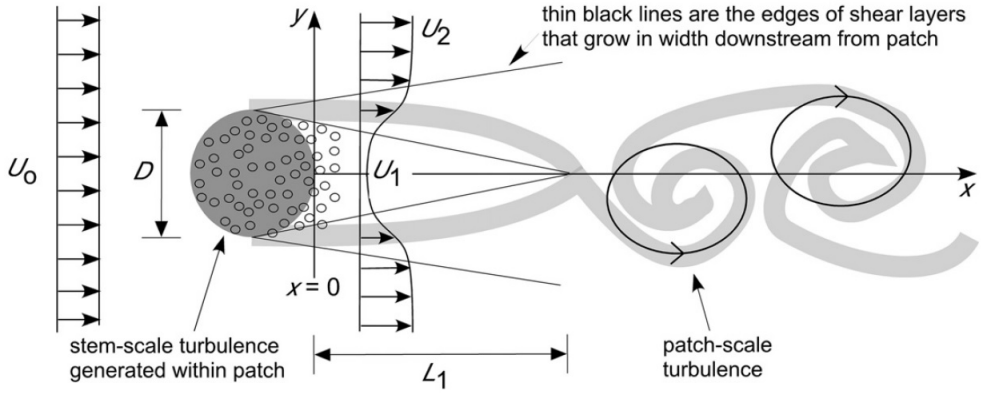

Fig. 1 – When the incoming flow, with velocity U_0, reaches a porous patch of diameter D, it is partly diverted with elevated velocity U_2 around the patch, and partly reduced to velocity U_1 behind the patch. The length L_1 refers to the steady wake. Image extracted from Follett and Nepf (2012)[7].

2 Methods

The model geometry consists of a channel reach containing a vegetation patch (Fig. 2). The circular patch has diameter D = 22 cm and is composed of 37 cylinders of diameter d = 0.64 cm that were arranged in square arrays, such that the frontal area per unit volume a was equal to 0.06 cm^{-1} and the solid volume fraction φ was equal to 0.03. The cylinders represent the vegetation stems. The flow blockage of the patch is aD = 1.32, a low value typical of sparse patches [10][11]. The patch is emergent, i.e., the rigid stems occupy the entire water depth. The patch was placed in the middle of a rectangular channel, which measures 550 cm in length and 120 cm in width. The width is the same one of the flume used by Follett and Nepf (2012)[7], who did not observe the influence of the walls on their experiments. The channel inlet is 12D upstream of the patch, far enough to allow the full development of the flow. The channel outlet is 12D downstream of the patch, and should be far enough to allow the steady wake to form behind the patch. The water depth is 12 cm, followed by 3 cm of air above it. The x-axis points to the longitudinal direction, the y-axis points to the vertical direction, and the z-axis points to the transverse direction. The correspondent velocities are (u, v, w), respectively. The origin (x, y, z = 0) is at the upfront border of the patch, at the bottom of the channel.

For boundary conditions, the inlet was treated as mass-flow inlet, where a uniform velocity of U_0 = 0.3 m/s was defined for both air and water in terms of mass flow rate ($\dot{m}_{water}$ = 43.1224 kg/s, $\dot{m}_{air}$= 0.01323 kg/s). The outlet wastreated as outflow. The bottom of the channel, the side walls and the stem cylinders were treated as walls, assuming no-slip condition. The atmosphere, at the top of the channel, was defined as symmetry, with zero normal velocities and zero normal gradients of all variables.

The computational mesh was generated at ICEM-CFD. The multiblock, unstructured approach was used, and the elements were hexahedral (Fig. 3a). In the horizontal plane, the geometry was divided into elements measuring 1 cm x 1 cm outside the patch (Fig. 3b). To refine the mesh inside the patch, O-grid blocks were created around the stem cylinders, which were 3.3 cm distant between each other. The edges of the O-grid blocks

pointing towards the cylinders were divided into 0.5-cm long segments (Fig. 3c). In the vertical axis, the elements measured 0.25 cm from 0 to 1 cm, and 1.4 cm above 1 cm (Fig. 3d). This refinement was made to better capture the flow velocity close to the bottom. In total, the mesh contained 1,002,780 nodes and 1,085,960 elements. Due to computational limitation, further refinement in the mesh was not implemented, but as it will be described later, the results agreed with experimental data.

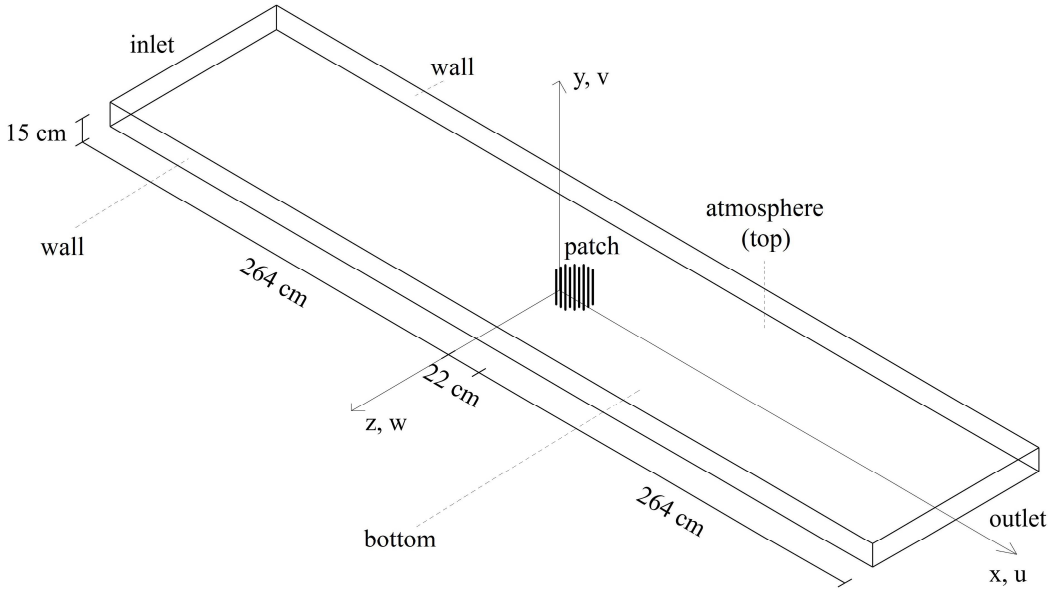

Fig. 2 – Geometry of the model. The patch was placed in the middle of the channel, and it was composed of 37 cylinders arranged in square arrays, such that each cylinder's center was 3.3 cm distant from its neighbors. A uniform flow of U_0 enters the domain through the inlet, in the form of mass flow rate, and leaves at the outlet. The water and air zones were not defined at the geometry, but rather during the setup of the solver.

The governing equations, which were integrated over each control volume, were formulated according to the Reynolds-Averaged Navier-Stokes (RANS) approach. In order to simulate the open channel flow, the Volume of Fluid (VOF) method was used. This method makes it possible to simulate the motion of two or more immiscible fluids by solving a single momentum equation throughout the domain, which in this case consists of water and air. The volume fraction of each fluid is tracked by solving the continuity equation for the volume fraction of one of the phases (air), and then computing the volume fraction of the other phase (water). This way, the free surface of the water can be tracked, and the velocity and pressure fields of the water can be simulated.

The single momentum equation, which governs the motion of the water-air mixture, is given by

$$(\rho u_i)_{,t} + (\rho u_i u_j)_{,j} = -p_{,i} + \rho f_i + T_{ij,j} \quad (1)$$

where ρ is the macroscopic density of the mixture, being computed through the relation

$$\rho = (1 - \alpha_a)\tilde{\rho}_w + \alpha_a \tilde{\rho}_a \quad (2)$$

where $\tilde{\rho}_w$ and $\tilde{\rho}_a$ are, respectively, the microscopic densities of water and air, α_a is the volume fraction of air, u_i is the i-th component of the velocity (which is shared between the phases), p is the pressure of fluid, f_i is the i-th component of the mean force vector, and T_{ij} is the Reynolds stress tensor, which is related to the strain-rate tensor, D_{ij}, and the turbulent kinetic energy, k, through the relation

$$T_{ij} = 2\nu_t D_{ij} - \frac{2}{3} k \delta_{ij} \quad (3)$$

where ν_t is the kinematic eddy viscosity, and δ_{ij} is the Kronecker symbol.

The volume fraction of air, α_a, is computed by solving its continuity equation:

$$(a\tilde{\rho}_a)_{,t} + (a\tilde{\rho}_a u_i)_{,j} = 0 \quad (4)$$

Differently from the air phase, a volume fraction equation is not solved for the water phase. Instead, the volume fraction of water, α_w, is computed based on the following constraint:

$$\alpha_a + \alpha_w = 1 \quad (5)$$

The k-ε model was used in order to account for turbulence [18]. A single set of transport equations is solved for the turbulent kinetic energy, k, and its dissipation rate, ε, which are shared between the water and air phases:

$$(\rho k)_{,t} + (\rho k u_i)_{,i} = \left[\left(\mu + \frac{\mu_t}{\sigma_k}\right)\frac{\partial k}{\partial x_j}\right]_{,j} + G_k - \rho\varepsilon - Y_M \quad (6)$$

$$(\rho \varepsilon)_{,t} + (\rho \varepsilon u_i)_{,i} = \left[\left(\mu + \frac{\mu_t}{\sigma_\varepsilon}\right)\frac{\partial \varepsilon}{\partial x_j}\right]_{,j} + C_{1\varepsilon}\frac{\varepsilon}{k}G_k - C_{2\varepsilon}\rho\frac{\varepsilon^2}{k} \quad (7)$$

where G_k represents the generation of turbulence kinetic energy due to the mean velocity gradients, Y_M represents the contribution of fluctuating dilatation in compressible turbulence due to the overall dissipation rate, $C_{1\varepsilon}$ and $C_{2\varepsilon}$ are constants, and σ_k and σ_ε are the turbulent Prandtl numbers for k and ε, respectively. The turbulent viscosity μ_t is obtained through Eq. 8:

$$\mu_t = \rho C_\mu \frac{k^2}{\varepsilon} \quad (8)$$

where C_μ is a constant. The default values $C_{1\varepsilon}$ = 1.44, $C_{2\varepsilon}$ = 1.92, C_μ = 0.09, σ_k = 1.0 and σ_ε = 1.3 were used in the simulations. As with the density ρ, the other properties that appear in the transport equations (μandμ_t) are determined by the presence of the phases in each control volume:

$$\mu = (1 - \alpha_a)\tilde{\mu}_w + \alpha_a\tilde{\mu}_a \quad (9)$$

$$\mu_t = (1 - \alpha_a)\tilde{\mu}_{t_w} + \alpha_a\tilde{\mu}_{t_a} \quad (10)$$

For the pressure-velocity coupling, the Semi Implicit Method for Pressure-linked Equations (SIMPLE) algorithm was employed.

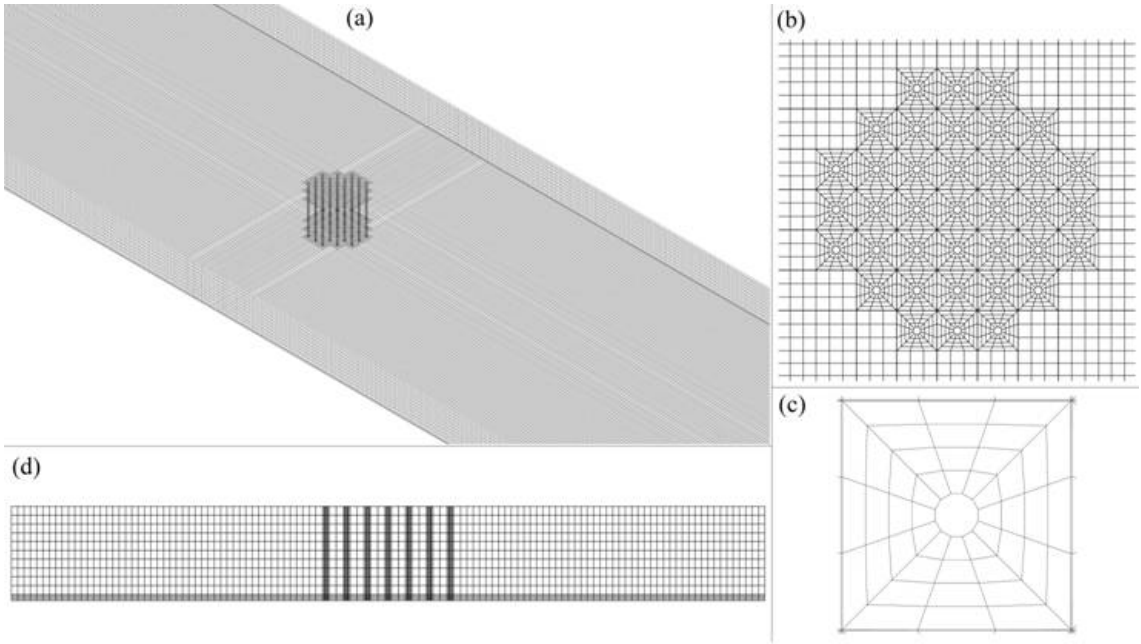

Fig. 3 – Computational mesh of the model. In (a), the mesh is seen throughout the domain (isometric view); in (b), plan view of the mesh at the patch, where O-grid blocks were created around the cylinders; in (c), detail of the mesh around one cylinder stem, which is at the center; in (d), cross-section view of the mesh at x = 0, where the bottom was refined.

3 Results

The simulation was performed for approximately 75 seconds in the model, after the solution reached convergence. The velocity profiles of u/U_0 at the patch centerline (z/D = 0) became very similar when the time was approximately equal to 60 seconds, indicating that the flow field reached a constant behavior at this time. Thus, the results presented here were obtained for t = 60 s, and assume that they represent the behavior of the flow for longer periods of time.

As expected, the patch partially obstructed the water passage, changing the flow patterns in the

channel (Fig. 4). Behind the patch (x/D> 1), at the patch centerline (z/D = 0), the flow was reduced to approximately 60% of the initial velocity U_0, and that reduction persisted along the channel length, with a timid velocity recovery at the end. Differently, a peak of the lateral velocity w was observed at the patch edge (z/D = 0.5) to values near 16% of U_0, which reflects the acceleration of the flow that was diverted laterally.

When comparing with the experimental data of Zong and Nepf (2012) [10], the numerical results tend to underestimate the velocity values upstream of the patch and right behind the patch (0 <x/D<2). One way to improve the numerical fit upstream of the patch can be refining the mesh in this region. Behind the patch, we suspect that the difference between the numerical and experimental data may be due to the cylinder arrangement. In the numerical model, one row of cylinders were positioned at the patch centerline (z/D = 0), such that the center of the cylinders coincided with the patch centerline. It means that the velocity profile behind the patch captured the wake of the last cylinder, where the velocity is known to be the lowest. In the work of Zong and Nepf (2012) [10], it is not possible to address if the stem cylinders were positioned in the same way. It might had happened that the measurement of Zong and Nepf (2012) [10] was made in between cylinders, and not behind one cylinder, and so the velocity measured there was higher than in the numerical model. Nevertheless, the numerical data show a good agreement, following the behavior of the flow velocity along the x-axis.

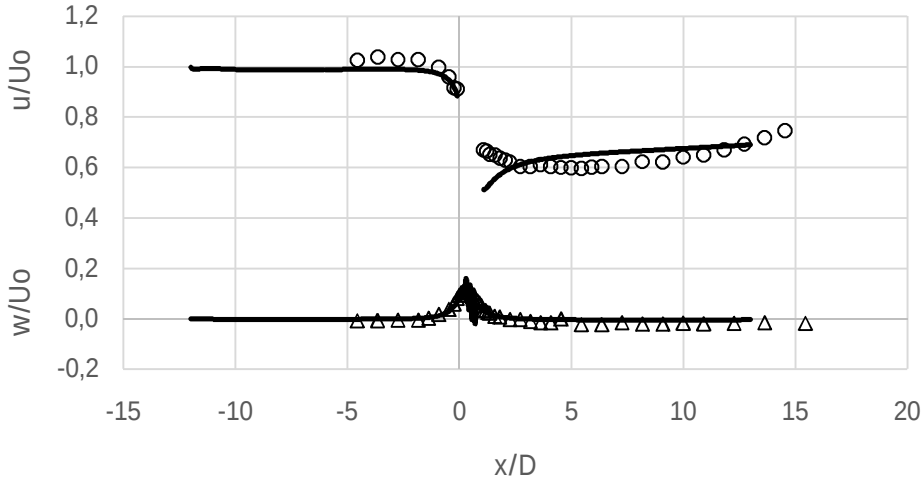

Fig. 4 – Depth-averaged velocity profiles of u/U_0 at the patch centerline (z/D = *0*), and w/U_0 at patch edge (z/D = 0.5) for t = 60 s. The patch was placed between x/D = 0 and x/D = 1. In comparison, the experimental data from Zong and Nepf (2012)[10] are shown as open symbols, while the numerical data are represented as lines. The profiles were obtained from the average of 9 points along the water depth, at the cell center of the grid elements.

Additionally to the velocity profiles, the patch created a new configuration of the flow field (Fig. 5). The patch is in the middle of the channel; regions in red indicate increased velocity, and regions in green and blue indicate that the velocity was reduced there. Two regions of increased velocity were formed around the patch, and they extended downstream of the channel, enclosing in between the quieter water of the steady wake that was formed behind the patch. Notice that the flow started to decelerate a little upstream of the patch (the yellow region in the front border of the patch). This is in agreement with experimental data from Chen et al. (2012) [11], who observed this upstream flow adjustment distance.

At several cross-sections of the channel, the velocity field was obtained (Fig. 6). Again, the red regions show accelerated flow, and blue and green regions show decelerated flow. Notice that before the patch (x/D = -1), the flow was practically constant, but once it reached the patch, the flow pattern started to change. The flow separation seen in the horizontal plane (Fig. 5) was also observed along the water depth, as the velocity behind the patch was reduced (green regions in Fig. 6), while the lateral regions were accelerated (Fig. 6, in red and orange). Moreover, inside the lateral regions there can be noticed a velocity gradient, as the velocity decreased from the central part to the adjacency, towards the channel walls and the bottom. This can indicate that the patch had a three-dimensional effect on the flow, additionally to the well-studied horizontal effects. Because the patch was sparse, with a low solid volume fraction of φ =

0.03, the interaction between the wakes of the stem cylinders were weak, and thus they did not induce wake billows [19].

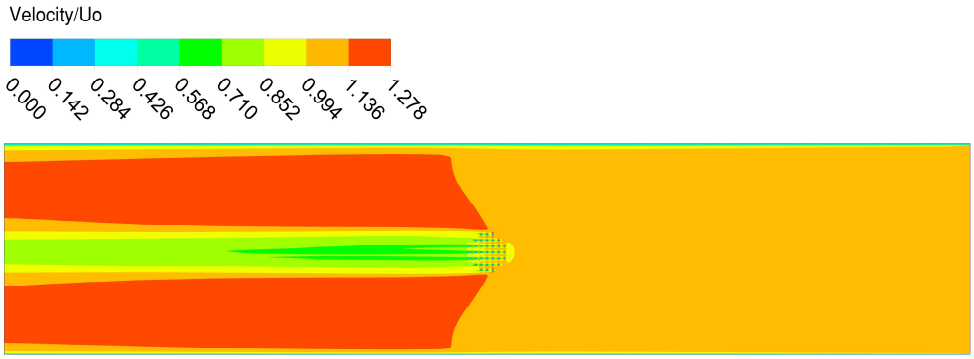

Fig. 5 – Contour map of the dimensionless velocity in the channel at mid-depth (plan view). The flow goes from right to left. The patch can locally change the flow pattern at a downstream length of 12 times its size.

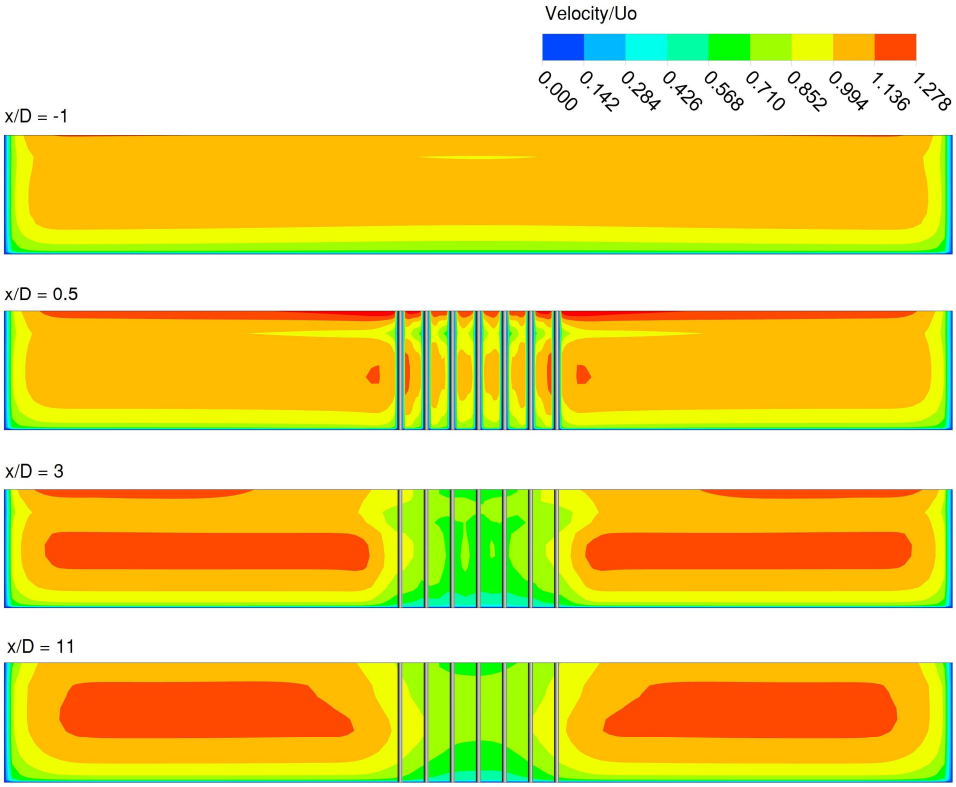

Fig. 6 – Velocity fields at different cross-sections of the channel. Before the patch (*x/D* = -1), the flow is undisturbed; at the patch (*x/D* = 0.5), the flow reaches the stem cylinders, which start to change the initial flow pattern; downstream of the patch (*x/D* = 3 and 11), the flow is organized in three distinct regions of velocity.

The free surface was defined for the water volume fraction equal to 0.5 [20] (Fig. 7). Regions in red indicate a water level increase, and regions in blue and green indicate that the water level decreased. Notice that the free surface increased in front of the cylinders, at the front border of the patch (*x/D* = 0), and decreased behind them. Then, the flow reached the next row of stem cylinders, elevating when it hit the cylinders, and decreasing its surface behind them. This elevation was not sufficient to recover the upstream water level, and consecutively, the water surface decreased from one row of cylinders to the next. It can be seen, thus, that the sum of the effects of the cylinders built the patch ability in disturbing the free surface.

The same phenomena was observed from the lateral view of the patch (Fig. 8a). When the flow hit the cylinders, it was blocked, losing velocity and elevating the water surface. Behind the cylinders, a small water depression was observed, as these were

the regions of stem-scale wakes, with reduced velocity. This is in agreement, for instance, with the study of Salaheldin et al. (2004) [21], who simulated the flow passing around a bridge pier. As the flow passed from one cylinder to the next, at a downstream position, the water surface was slowly, but continuously decreased. Then, the free surface recovered to its initial level about 5 cm downstream of the last cylinder. Between the first (most upstream) and the last (most downstream) cylinder of the patch, the difference in the free surface was 0.46 cm, which represented 3.83% of the total water depth. In the cross-section view of the channel (Fig. 8b), the free surface increased outwards from the patch edge, and towards the channel walls. The difference from the initial water level was 0.09 cm, representing 0.75% of the total water depth.

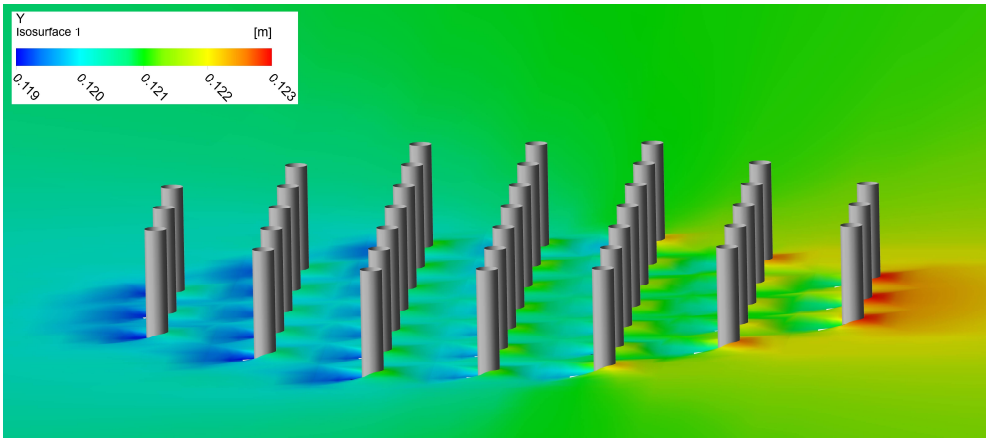

Fig. 7 – Resultant free surface at the patch. The flow goes from right to left. The water undulates when it passes through the patch. The free surface was defined for water volume fraction = 0.5.

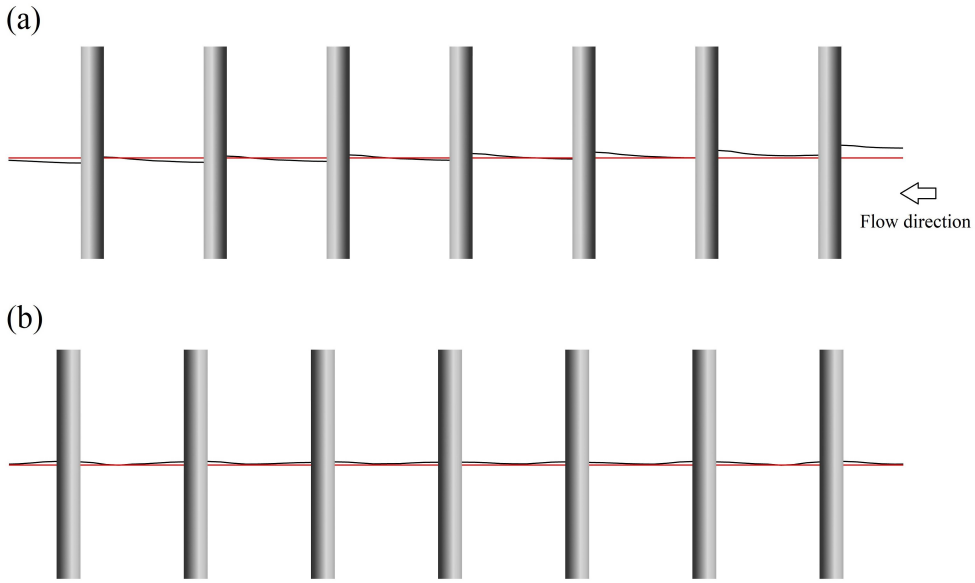

Fig. 8 – (a) Lateral view of the channel, at patch centerline (z/D = 0). The resultant free surface (black line) is compared with the initial free surface (red line). The patch induced undulations on the free surface, where the water level increased just before the first cylinder, and decreased after the last cylinder, recovering the initial level further downstream. (b) Cross-section view of the channel, at patch center (x/D = 0.5). The free surface increased at the edges of the patch.

It can be seen that the effect of the patch on the free surface was small, which is justified by the patch being sparse, its diameter being small, and the flow velocity being low. Bigger, denser patches will affect the free surface more significantly, as well as channels with faster flows. For instance, Naden et al. (2006) [6] measured the water depth in several cross-sections of a river reach in UK, and reported that the growth and spread of vegetation patches in the river caused an increase of the water depth to values close to twice the initial depth, in some profiles. Consequently, as possible overtopping of

the vegetation and overbanking can occur, it becomes important to take the free surface into account in such cases, using the three-dimensional approach in computational models (e.g., Cannata et al., 2017) [22], additionally to the two-dimensional aspects of the flow.

4 Conclusion

In this study, the hydrodynamic interactions between the flow and a vegetation patch in a channelwere simulated in a CFD, 3-D model. The simulation was performed with the RANS equations, and the free surface was represented through the VOF model. The patch was able to create three distinct flow regions along the water depth: two regions of higher velocity around the patch, and one region of reduced velocity in the wake of the patch. Moreover, the patch disturbed the initial water, creating a level difference upstream and downstream of it, and a level increase towards the channel walls. For future studies, it would be interesting to include the sediment phase to the model, and thus take into account the effects of the patch on sediment transport and bed morphology change of the channel.

Acknowledgments

Taís N. Yamasaki would like to thank Fundação de Apoioao Desenvolvimento do Ensino, Ciência e Tecnologia do Estado de Mato Grosso do Sul (FUNDECT) for support given to her with the program Mobility Confap Italy.

References:

[1] Wilcock, R.J., Champion, P.D., Nagels, J.W. & Crocker, G.F., The influence of aquatic macrophytes on the hydraulic and physico-chemical properties of a New Zealand lowland stream, *Hydrobiologia*, Vol.416, 1999, pp. 203-214.

[2] van Katwijk, M.M., Bos, A.R.,Hermus, D.C.R. & Suykerbuyk, W., Sediment modification by seagrass beds: muddification and sandification induced by plant cover and environmental conditions, *Estuarine, Coastal and Shelf Science*, Vol.89, No.2, 2010, pp. 175-181.

[3] Bouma, T.J., van Duren, L.A., Temmerman, S., Claverie, T., Blanco-Garcia, A., Ysebaert, T. & Herman, P.M.J., Spatial flow and sedimentation patterns within patches of epibenthic structures: combining field, flume and modelling experiments, *Continental Shelf Research*, Vol.27, No.8, 2007, pp. 1020-1045.

[4] Tal, M. & Paola, C., Dynamic single-thread channels maintained by the interaction of flow and vegetation, *The Geological Society of America*, Vol.35, No.4, 2007, pp. 347-350.

[5] Gurnell, A., Plants as river systems engineers, *Earth Surface Processes and Landforms*, Vol.39, 2014, pp. 4-25.

[6] Naden, P., Rameshwaran, P., Mountford, O. & Robertson, C., The influence of macrophyte growth, typical of eutrophic conditions, on river flow velocities and turbulence production, *Hydrological Processes*, Vol.20, 2006, pp. 3915-3938.

[7] Follett, E.M. & Nepf, H.M., Sediment patterns near a model patch of reedy emergent vegetation, *Geomorphology*, Vol.179, 2012, pp. 141-151.

[8] Ortiz, A.C., Ashton, A. & Nepf, H.M., Mean and turbulent velocity fields near rigid and flexible plants and the implications for deposition, *Journal of Geophysical Research: Earth Surface*, Vol.118, 2013, pp. 2585-2599.

[9] Shi, Y., Jiang, B. & Nepf, H.M., Influence of particle size and density, and channel velocity on the deposition patterns around a circular patch of model emergent vegetation, *Water Resources Research*, Vol.52, 2016, pp. 1044-1055.

[10] Zong, L. & Nepf, H.M., Vortex development behind a finite porous obstruction in a channel, *Journal of Fluid Mechanics*, Vol.691, 2012, pp. 368-391.

[11] Chen, Z., Ortiz, A., Zong, L. & Nepf, H.M., The wake structure behind a porous obstruction and its implications for deposition near a finite patch of emergent vegetation, *Water Resources Research*, Vol.48, 2012, pp. 1-12.

[12] Nepf, H.M., Hydrodynamics of vegetated channels, *Journal of Hydraulic Research*, Vol.50, 2012, pp. 262-279.

[13] Kondziolka, J.M. & Nepf, H.M., Vegetation wakes and wake interaction shaping aquatic landscape evolution, *Limnology and Oceanography: Fluids and Environments*, Vol.4, 2014, pp. 106-119.

[14] de Lima, P.H.S., Janzen, J.G. & Nepf, H.M., Flow patterns around two neighboring patches of emergent vegetation and possible implications for deposition and vegetation growth, *Environmental Fluid Mechanics*, Vol.15, 2015, pp. 881-898.

[15] Cannata, G., Lasaponara, F. & Gallerano, F., Non-linear Shallow Water Equations numerical

integration on curvilinear boundary-conforming grids, *WSEAS Transactions on Fluid Mechanics*, Vol.10, 2015, pp. 13-25.

[16] Gallerano, F., Cannata, G. & Lasaponara, F., Numerical simulation of wave transformation, breaking run-up by a contravariant fully nonlinear Boussinesq model, *Journal of Hydrodynamics B*, Vol.28, 2016, pp. 379-388.

[17] Gallerano, F., Cannata, G. & Lasaponara, F., A new numerical model for simulations of wave transformation, breaking and longshore currents in complex coastal regions, *International Journal for Numerical Methodsin Fluids*, Vol.80, 2016, pp. 571-613.

[18] Gallerano, F., Pasero, E. & Cannata, G., A dynamic two-equation sub grid scale model, *Continuum Mechanics and Thermodynamics*, Vol.17 (2), 2005, pp. 101-123.

[19] Chang, Kyoungsik & Constantinescu, G., Numerical investigation of flow and turbulence structure through and around a circular array of rigid cylinders, *Journal of Fluid Mechanics*, Vol.776, 2015, pp. 161-199.

[20] Dommermuth, D.G., O'Shea, T.T., Wyatt, D.C., Ratcliffe, T., Weymouth, G.D., Hendrikson, K.L., Yue, D.K.P., Sussman, M., Adams, P. & Valenciano, M., An application of cartesian-grid and Volume-of-Fluid methods to numerical ship hydrodynamics, *9th International Conference on Numerical Ship Hydrodynamics, Ann Arbor, Michigan*, 2007.

[21] Salaheldin, T.M., Imran, J. & Chaudhry, M.H., Numerical modeling of three-dimensional flow field around circular piers, *Journal of Hydraulic Engineering*, Vol.130, No.2, 2004, pp. 91-100.

[22] Cannata, G., Petrelli, C., Barsi, L., Camilli, F. & Gallerano, F., 3D free surface flow simulations based on the integral form of the equations of motion, *WSEAS Transactions on Fluid Mechanics*, Vol.12, 2017, pp. 166-175.